International Journal of Future Generation Communication and Networking
Vol.7, No.4 (2014), pp.183-194
http://dx.doi.org/10.14257/ijfgcn.2014.7.4.17

Full-wave Analysis of Rectangular Microstrip Antenna Printed on Electric-Magnetic Uniaxial Anisotropic Substrates

Mourad Hassad, Akram Soufiane Boughrara and Tarek Fortaki

Department of Electronics, University of Batna, Batna 05000, Algeria
hassadmourad@gmail.com

Abstract

This paper presents the resonant characteristics of rectangular microstrip antenna printed on anisotropic substrate. The anisotropic substrates are characterized by both permittivity and permeability tensors. The analysis is performed in the spectral domain method by using Green's function technique. Numerical results concerning the effects of electric anisotropy and antennas parameters on the resonant characteristics of rectangular microstrip antenna are presented and discussed. Results are compared with previously published data and are found to be in good agreement.

Keywords: *spectral domain method; electric & magnetic anisotropic substrates; Galerkin moment method*

1. Introduction

Microstrip patch antennas (MPAs) are used in the wide range of applications, due to many attractive features. The features, including their very low profile, low cost, light weight, conformal structure, mechanical ruggedness, and ease in fabrication and integration with solid-state devices, make them important, especially for applications mounted on the exterior of aircraft and spacecraft or incorporated into mobile radio communications devices [1-3].

MPAs comprise narrow bandwidth that is approximately 1-5%, which is the most major limiting factor for its widespread applications [1]. The conventional microstrip antenna is a metallic patch printed on a thin, grounded isotropic dielectric substrate [4]. Even though conventional patch antennas have the major weaknesses of narrowband and low gain, there are several techniques to overcome these weaknesses [1]. This warrants new research on possible methods of performance enhancement, employing other types of substrate materials and antenna geometries [4-5].

However, there has been very little research into using anisotropic materials as substrates [6-11]. By introducing a variety of anisotropic dielectrics into multilayered microstrip antennas, some of those unwanted characteristics of conventional antenna could potentially be eliminated or improved [4]. The use of anisotropic dielectrics may improve the frequency range of these devices, and gives more accuracy and flexibility in the design [12]. With the increasing complexity of geometry and material property, designing these antennas requires more and more dedicated and sophisticated computer aided-design (CAD) tools to predict the characteristics. The method of moments (MoM) has been proven to be one of the most powerful CAD tools for solving this class of problems. By now, a number of microstrip antennas with anisotropic substrate have been investigated using the MoM based spectral domain analysis method [6-8].

The effects of uniaxial anisotropy on the resonant frequency and the bandwidth of a monolayer microstrip antenna have been studied in several works, for a rectangular patch in

ISSN: 2233-7857 IJFGCN

[6-8], and for a circular patch in [9-11], where the positive and negative uniaxial anisotropies were considered. However, the studies were limited to the case of the effect of the electric uniaxial anisotropy on the resonant characteristics of microstrip patch antenna. In this paper the effects of the both electric and magnetic uniaxial anisotropy, in the substrate on the resonant characteristics of the rectangular microstrip patch antenna are investigated. The paper is organized as follows. In Section 2, the derivations of the electric uniaxial Green's function in spectral form, the associated moment method analysis for the complex resonant frequency of the printed antenna are presented. The calculation is performed with vector Fourier transforms which gives rise to a diagonal form of the Green's function. The effects of antenna parameters on the resonant characteristics of rectangular microstrip antenna are investigated in section 3. Variations in the permittivity perpendicular to the optical axis of the dielectric and along this axis are considered. Concluding remarks are summarized in Section 4.

2. Spectral Domain Formulation

The geometry under consideration is illustrated in Figure 1. A rectangular patch with dimensions (a, b) along the two axes (x, y), respectively, is printed on a grounded dielectric slab of thickness d, characterized by the free-space permeability μ_0 and the permittivity ε_0, ε_r (ε_0 is the free-space permittivity and the relative permittivity ε_r can be complex to account for dielectric loss).

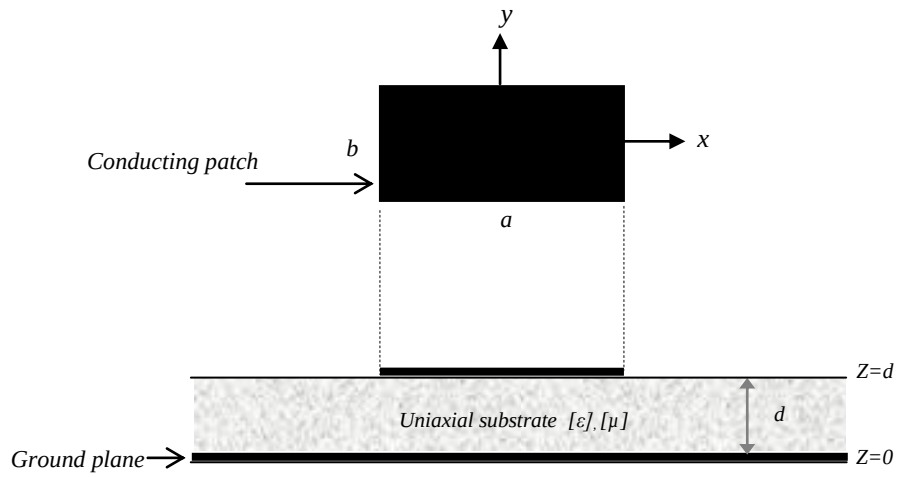

Figure 1. Geometrical Structure of a Rectangular Microstrip Antenna

All fields and currents are time harmonic with the $e^{i\omega t}$ time dependence suppressed. The anisotropic substrate layer is characterized by a permittivity and permeability tensors of the form

$$\bar{\bar{\varepsilon}} = \varepsilon_0 \begin{bmatrix} \varepsilon_x & 0 & 0 \\ 0 & \varepsilon_x & 0 \\ 0 & 0 & \varepsilon_z \end{bmatrix} \quad (1)$$

$$\bar{\mu} = \mu_0 \begin{bmatrix} \mu_x & 0 & 0 \\ 0 & \mu_x & 0 \\ 0 & 0 & \mu_z \end{bmatrix} \tag{2}$$

The transverse fields inside the anisotropic substrate ($0<z<d$) can be obtained via the inverse vector Fourier transform as

$$\mathbf{E}(r_s, z) = \begin{bmatrix} E_x(\mathbf{r}_s, z) \\ E_y(\mathbf{r}_s, z) \end{bmatrix} = \frac{1}{4\pi^2} \int_{-\infty}^{+\infty} \int_{-\infty}^{+\infty} \bar{\mathbf{F}}(\mathbf{k}_s, \mathbf{r}_s) \cdot \mathbf{e}(\mathbf{k}_s, z)\, dk_x\, dk_y \tag{3}$$

$$\mathbf{H}(\mathbf{r}_s, z) = \begin{bmatrix} H_y(\mathbf{r}_s, z) \\ -H_x(\mathbf{r}_s, z) \end{bmatrix} = \frac{1}{4\pi^2} \int_{-\infty}^{+\infty} \int_{-\infty}^{+\infty} \bar{\mathbf{F}}(\mathbf{k}_s, \mathbf{r}_s) \cdot h(\mathbf{k}_s, z)\, dk_x\, dk_y \tag{4}$$

where $\bar{\mathbf{F}}(\mathbf{k}_s, \mathbf{r}_s)$ is the kernel of the vector Fourier transform [13-15],

$$\bar{\mathbf{F}}(\mathbf{k}_s, \mathbf{r}_s) = \frac{1}{k_s} \begin{bmatrix} k_x & k_y \\ k_y & -k_x \end{bmatrix} e^{i\mathbf{k}_s \cdot \mathbf{r}_s}, \mathbf{r}_s = \hat{\mathbf{x}}x + \hat{\mathbf{y}}y,\ \mathbf{k}_s = \hat{\mathbf{x}}k_x + \hat{\mathbf{y}}k_y,\ k_s = |\mathbf{k}_s| \tag{5}$$

and

$$\mathbf{e}(\mathbf{k}_s, z) = \mathbf{A}(\mathbf{k}_s) e^{-i\bar{\mathbf{k}}_z z} + \mathbf{B}(\mathbf{k}_s) e^{i\bar{\mathbf{k}}_z z} \tag{6}$$

$$\mathbf{h}(\mathbf{k}_s, z) = \bar{\mathbf{g}}(\mathbf{k}_s) \cdot \begin{bmatrix} \mathbf{A}(\mathbf{k}_s) e^{-i\bar{\mathbf{k}}_z z} - \mathbf{B}(\mathbf{k}_s) e^{i\bar{\mathbf{k}}_z z} \end{bmatrix} \tag{7}$$

In Eqs. 6 and 7, $\tilde{E}_z(\mathbf{k}_s, z)$ and $\tilde{H}_z(\mathbf{k}_s, z)$ are the scalar Fourier transforms of $E_z(\mathbf{r}_s, z)$ and $H_z(\mathbf{r}_s, z)$, respectively. $\mathbf{A}$ and $\mathbf{B}$ are two-component unknown vectors and

$$\bar{\mathbf{g}}(\mathbf{k}_s) = \mathbf{diag} \begin{bmatrix} \frac{\omega\varepsilon_0\varepsilon_x}{k_z^e}, \frac{k_z^h}{\omega\mu_0\mu_x} \end{bmatrix},\ \bar{\mathbf{k}}_z = diag\ \left[k_z^e, k_z^h\right] \tag{8}$$

with $k_0^2 = \omega^2 \varepsilon_0 \mu_0$ k_z^e and k_z^h are , respectively, propagation constants for TM and TE waves in the uniaxial substrate they are given by

$$k_z^e = \sqrt{\frac{\varepsilon_x}{\varepsilon_z}} (\mu_x \varepsilon_z k_0^2 - k_s^2)^{\frac{1}{2}},\ k_z^h = \sqrt{\frac{\mu_x}{\mu_z}} (\mu_z \varepsilon_x k_0^2 - k_s^2)^{\frac{1}{2}},\ k_0^2 = \omega^2 \varepsilon_0 \mu_0 \tag{9}$$

Writing Eqs. 4 and 5 in the planes $z = 0$ and $z = d$, and by eliminating the unknowns $\mathbf{A}$ and $\mathbf{B}$, we obtain the matrix form

$$\begin{bmatrix} \mathbf{e}(\mathbf{k}_s, d^-) \\ \mathbf{h}(\mathbf{k}_s, d^-) \end{bmatrix} = \bar{\mathbf{T}} \cdot \begin{bmatrix} \mathbf{e}(\mathbf{k}_s, 0^+) \\ \mathbf{h}(\mathbf{k}_s, 0^+) \end{bmatrix} \tag{10}$$

with

$$\overline{\mathbf{T}} = \begin{bmatrix} \overline{\mathbf{T}}^{11} & \overline{\mathbf{T}}^{12} \\ \overline{\mathbf{T}}^{21} & \overline{\mathbf{T}}^{22} \end{bmatrix} = \begin{bmatrix} \overline{\mathbf{I}} \cos\overline{\boldsymbol{\theta}} & -\mathbf{i}\,\overline{\mathbf{g}}^{-1}\sin\overline{\boldsymbol{\theta}} \\ -\mathbf{i}\,\overline{\mathbf{g}}\sin\overline{\boldsymbol{\theta}} & \overline{\mathbf{I}}\cos\overline{\boldsymbol{\theta}} \end{bmatrix} \tag{11}$$

which combines $\mathbf{e}$ and $\mathbf{h}$ on both sides of the uniaxial layer as input and output quantities. In Eq. 12, $\theta = k_z d$ and $\overline{I}$ stands for the 2 x 2 unit matrix. The matrix $\overline{\mathbf{T}}$ is the matrix representation of the uniaxial layer in the (TM, TE) representation. The continuity equations for the tangential field components are

$$\mathbf{e}(\mathbf{k}_s, d^-) = \mathbf{e}(\mathbf{k}_s, d^+) = \mathbf{e}(\mathbf{k}_s, d) \tag{12}$$

$\tilde{\mathbf{J}}(\mathbf{k}_s)$ is the vector Fourier transform of current $\tilde{\mathbf{J}}(\mathbf{r}_s)$ on the patch, it accounts for the discontinuity of the tangential magnetic field at the interface *z=d*. δ_P is the Kronecker symbol, defined by [13]

$$\begin{bmatrix} \mathbf{e}(\mathbf{k}_s, d^+) \\ \mathbf{h}(\mathbf{k}_s, d^+) \end{bmatrix} = \overline{\mathbf{T}} \cdot \begin{bmatrix} \mathbf{e}(\mathbf{k}_s, 0^+) \\ \mathbf{h}(\mathbf{k}_s, 0^+) \end{bmatrix} - \begin{bmatrix} 0 \\ j(\mathbf{k}_s) \end{bmatrix} \tag{13}$$

In the unbounded air region above the top patch of the stacked structure $(d < z < \infty \text{ and } \varepsilon_r = 1)$ the electromagnetic field given by Eqs. 6 and 7 should vanish at $z \to +\infty$ according to Sommerfeld's condition of radiation, this yields

$$\mathbf{h}(\mathbf{k}_s, d^+) = \overline{\mathbf{g}}_0(\mathbf{k}_s) \cdot \mathbf{e}(\mathbf{k}_s, d^+) \tag{14}$$

where $\overline{\mathbf{g}}_0(\mathbf{k}_s)$ can be easily obtained from the expression of $\overline{\mathbf{g}}(\mathbf{k}_s)$ given in Eq. 5 by allowing $\varepsilon_x = \varepsilon_z = \varepsilon_r = 1$ and $\mu_x = \mu_z = \mu_r = 1$. The transverse electric field must necessarily be zero at the plane z = 0, so that we have

$$\mathbf{e}(\mathbf{k}_s, d^-) = \mathbf{e}(\mathbf{k}_s, d^+) = \mathbf{e}(\mathbf{k}_s, d) = 0 \tag{15}$$

From Eqs. 10-13, we obtain a relation among $j(\mathbf{k}_s)$ and $\mathbf{e}(\mathbf{k}_s, d)$ given by [14]

$$\mathbf{e}(\mathbf{k}_s, d) = \overline{\mathbf{G}}(\mathbf{k}_s) \cdot j(\mathbf{k}_s) \tag{16}$$

Where $\overline{\mathbf{G}}(\mathbf{k}_s)$ is the dydic Green's function in the vector Fourier transform domain, it is given by

$$\overline{\mathbf{G}}(\mathbf{k}_s) = \text{diag}\left[G^{11}, G^{22}\right] = \left[\overline{\mathbf{T}}^{22}(\overline{\mathbf{T}}^{12})^{-1} - \overline{\mathbf{g}}_0\right] \tag{17}$$

Using the technique known as the moment method, with weighting modes chosen identical to the expansion modes, Eqs. 15 and 16 are reduced to a system of linear equations which can be written compactly in matrix form as [14]

$$\overline{\mathbf{Z}} \cdot \mathbf{C} = \mathbf{0} \tag{18}$$

where $\overline{\mathbf{Z}}$ is the impedance matrix and the elements of the vector $\mathbf{C}$ are the mode expansion coefficients to be sought [13-15]. Note that each element of the impedance matrix

$\overline{\mathbf{Z}}$ is expressed in terms of a doubly infinite integral [13]. The system of linear equations given in Eq. 18 has non-trivial solutions when

$$det\ [\ \overline{\mathbf{Z}}(\omega)] = 0 \tag{19}$$

Eq. 26 is an Eigen equation for ω, from which the characteristics of the stacked structure of Figure 1 can be obtained. In fact, let $\omega = 2\pi(f_r + i f_i)$ be the complex root of Eq. 19. In that case, the quantity f_r stands for the resonant frequency, the quantity $BW = 2 f_i / f_r$ stands for the bandwidth and the quantity $Q = f_r/(2 f_i)$ stands for the quality factor.

Although the full-wave analysis can give results for several resonant modes [13, 15], only results for the TM_{01} mode are presented in this study. The basis functions for the following numerical calculations are selected to be sinusoidal functions of

$$J_{xk}(x,y) = \sin\left[\frac{k_1\pi}{a}(x+\frac{a}{2})\right]\cos\left[\frac{k_2\pi}{b}(y+\frac{b}{2})\right] \tag{20.a}$$

$$J_{ym}(x,y) = \sin\left[\frac{m_2\pi}{b}(y+\frac{b}{2})\right]\cos\left[\frac{m_1\pi}{a}(x+\frac{a}{2})\right] \tag{20.b}$$

Note that the modes are now identified by the integer doublet k_1k_2 (m_1m_2) instead of $k(m)$. This type of basis function is very appropriate for the vector Fourier transform domain analysis of rectangular microstrip patches for three reasons: they ensure a quick convergence of the Galerkin's method in the vector Fourier transform domain with respect to the number of basis functions, they lead to vector Fourier transform domain infinite integrals, which are amenable to asymptotic analytical integration techniques and their vector Fourier transforms can be obtained in closed form [13, 15].

3. Numerical Results and Discussion

In order to confirm the computation accuracy, our calculated resonant frequencies are compared with recently experimental and theoretical published data [17].

Table 1. Comparison of the Calculated Results of the Resonance Frequency with Measured Data for a Rectangular Microstrip Patch Antenna on Isotropic Substrate, with; *a*=25.08mm, *b*=15.438mm, $\varepsilon_x = \varepsilon_z = 2.2$, $\mu_x = \mu_z = 1$

d(mm)	**Resonant frequency f_r (GHz)**			
	Measured	**Calculated**		
	[17]	**[17]**	**[18]**	**Our results**
0.84	6.057	6.092	6.15	6.053
1.64	5.887	5.883	5.89	5.885

Table I summarizes the measured and computed resonant frequencies for different geometrical antenna.

In order to check the accuracy of the spectral domain method described in the previous section for electric anisotropic case, our results are compared with an experimental and theoretical values presented in the previous work [17, 19].

Table 2. Comparison of Calculated and Measured Resonant Frequencies, for a Rectangular Microstrip Patch in a Uniaxial Electric Anisotropic Substrate ($\varepsilon_x = 13.0$, $\varepsilon_z = 10.2$), $\mu_x = \mu_z = 1$

Input parameters			Resonant frequency f_r (GHz)			
			Measured	Calculated		
d (mm)	*a* (mm)	*b* (mm)	[19]	[19]	[17]	Our results
1.27	30	20	2.264	2.268	2.261	2.284
1.27	15	9.5	4.495	4.520	4.355	4.599
2.54	30	19	2.242	2.260	2.177	2.299

The resonant frequency and half-power bandwidth of the patch antenna against the substrate thickness are shown in Figures 2(a) and (b), where isotropic ($\varepsilon_x = \varepsilon_z = 2.43$), negative uniaxial anisotropic ($\varepsilon_x = 2.43$, $\varepsilon_z = 1.62$) and positive uniaxial anisotropic ($\varepsilon_x = 2.43$, $\varepsilon_z = 4.86$) substrates are considered. In Figure 2(a), the anisotropy is obtained by changing ε_z while keeping ε_x constant. The effect of the permittivity along the optical axis persists for low as well as for high substrate thicknesses. As for the bandwidth (Figure 2(b)), it is increased due to the negative uniaxial anisotropy and decreased due to the positive uniaxial anisotropy. When ε_x is changed and ε_z remains constant, the influence of the resonant frequency decreases with reductions in substrate thickness as shown in Figure 3(a). This influence tends to be neglected for lower substrate thickness. These behaviors agree very well with those reported for a various shapes patch antenna, by [6-11].

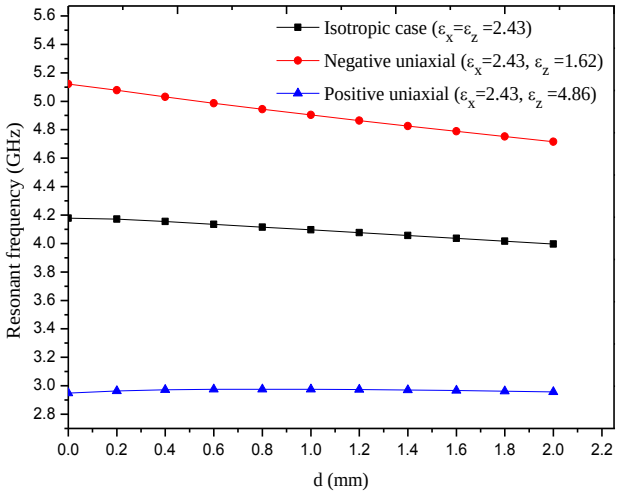

(a) Resonant Frequency.

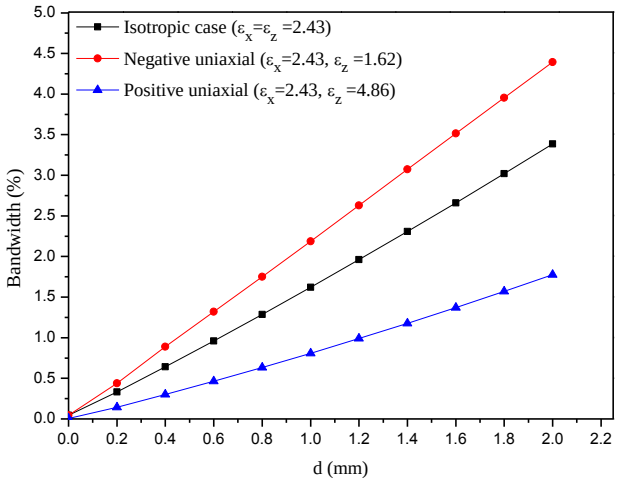

(b) Bandwidth.

Figure 2. Resonant Frequency and Bandwidth Versus the Substrate Thickness for Isotropic, Negative Uniaxial and Positive Uniaxial Electric Anisotropic Substrates When Changing ε_z ; $a = 19\ mm$, $b = 22.9\ mm$, $\mu_x = \mu_z = 1$: (A) Resonant Frequency, (b) Bandwidth

Figure 3(b) shows the results for the half-power bandwidth of the patch antenna. The positive uniaxial anisotropy slightly increases the half-power bandwidth, while the negative uniaxial anisotropy slightly decreases the half-power bandwidth. The variations of bandwidth due to the uniaxial anisotropy are also seen to increase when the substrate thickness is increased. We can conclude that the permittivity ε_z along the optical axis is the significant and most important factor in determination of the resonant frequency.

Now, the effects of uniaxial magnetic anisotropy on the resonant frequency and the bandwidth characteristics are shown in Figures 4 and 5.

Figure 4(a) show the influence of magnetic uniaxial anisotropy in the substrate on the resonant frequency, when we change the substrate thickness for different case; isotropic case $(\mu_x = \mu_z = 2.4)$; negative uniaxial anisotropy $(\mu_x = 4.8, \mu_z = 2.4)$ and positive uniaxial $(\mu_x = 1.2, \mu_z = 2.4)$ substrates, the magnetic anisotropy is obtained by changing μ_x while keeping μ_z constant. It is found that the resonant frequency is shifted to higher frequencies for the positive uniaxial case $(\mu_x = 1.2, \mu_z = 2.4)$ and, on other hand, is shifted to lower frequencies for the negative uniaxial case $(\mu_x = 4.8, \mu_z = 2.4)$. As for the half-power bandwidth (Figure 4(b)), it is increased due to the negative uniaxial anisotropy, and decreased due to the positive uniaxial anisotropy.

Figure 4(a) and 4(b) show the resonant frequency and bandwidth versus the substrate thickness for a rectangular microstrip patch antenna, where the cases of isotropy $(\mu_x = \mu_z = 2.4)$, negative anisotropy $(\mu_x = 2.4, \mu_z = 1.2)$, and positive anisotropy $(\mu_x = 2.4, \mu_z = 4.8)$ are presented. The magnetic anisotropy is obtained by changing μ_z while keeping μ_x constant. The values of resonant frequency and bandwidth of rectangular microstrip antenna for anisotropic cases are very close to the values of the isotropic case especially in the case of the positive uniaxial anisotropy.

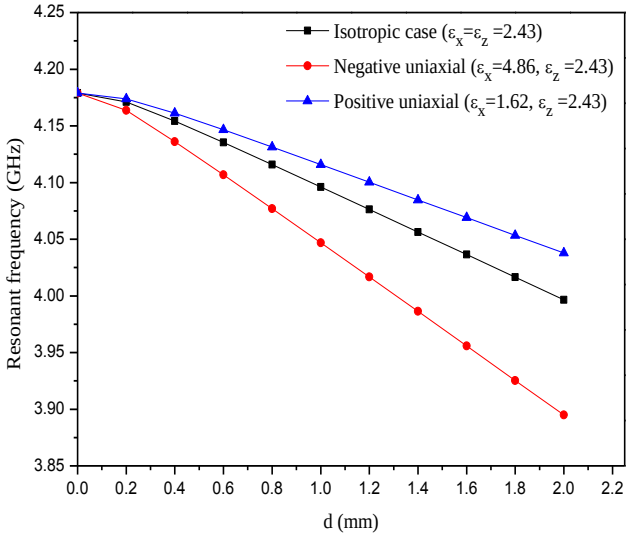

(a) Resonant frequency.

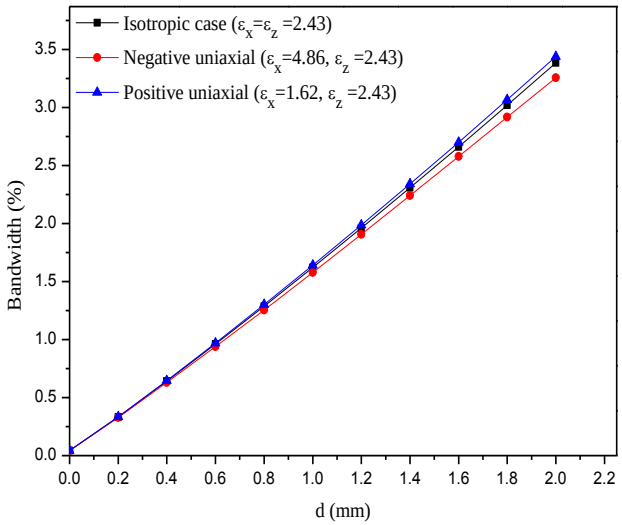

(b) Bandwidth.

Figure 3. Resonant Frequency and Bandwidth versus the Substrate Thickness for Isotropic, Negative Uniaxial and Positive Uniaxial Electric Anisotropic Substrates when Changing ε_x ; $a = 19\ mm$, $b = 22.9\ mm$, $\mu_x = \mu_z = 1$: (a) Resonant Frequency, (b) Bandwidth

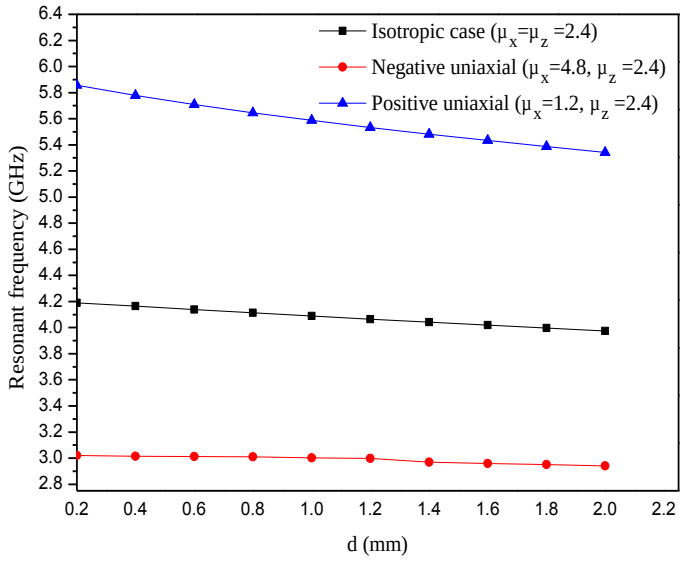

(a) Resonant Frequency.

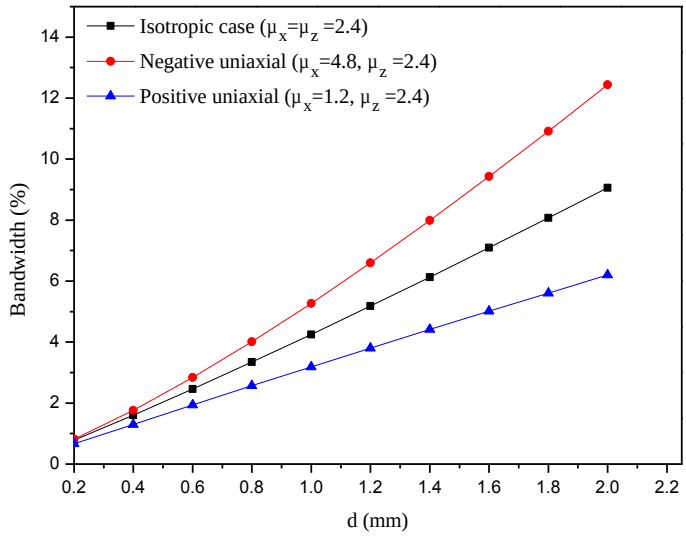

(b) Bandwidth.

Figure 4. Resonant Frequency and Bandwidth versus the Substrate Thickness for Isotropic, Negative Uniaxial and Positive Uniaxial Magnetic Anisotropic Substrates when Changing μ_x ; $a = 19\ mm$, $b = 22.9\ mm$, $\varepsilon_x = \varepsilon_z = 1$: (a) Resonant Frequency, (b) Bandwidth

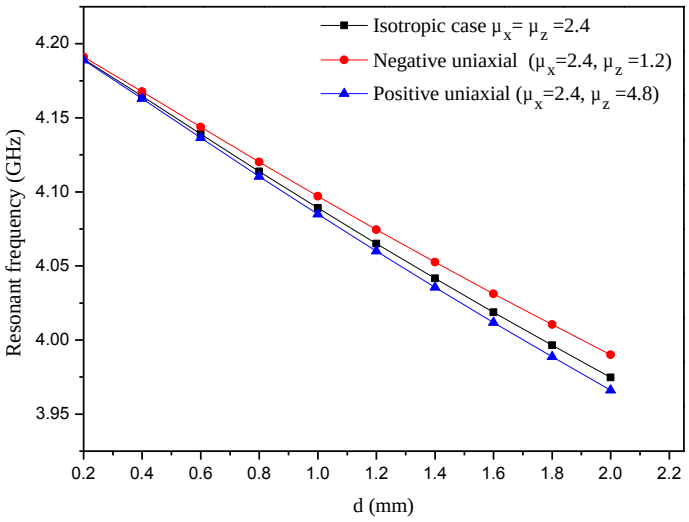

(a) Resonant frequency.

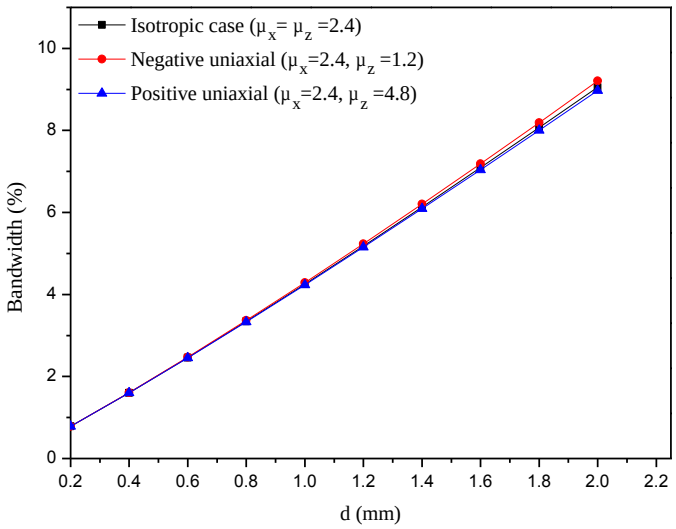

(a) Bandwidth.

Figure 5. Resonant Frequency and Bandwidth versus the Substrate Thickness for Isotropic, Negative Uniaxial and Positive Uniaxial Magnetic Anisotropic Substrates when Changing μ_z ; $a = 19\ mm$, $b = 22.9\ mm$, $\varepsilon_x = \varepsilon_z = 1$: (a) Resonant Frequency, (b) Bandwidth

The results are plotted in Figures 4, and 5. Whereas the antenna parameters (resonance frequency, bandwidth) do not vary significantly with the permeability variation along to the optical axis (μ_z), these are found to be strongly dependent with the permeability variation

perpendicular the optical axis (μ_x). Interesting enhancement of the bandwidth is obtained for the case of negative uniaxial anisotropy along the optical axis.

4. Conclusion

We have described an accurate analysis of rectangular microstrip antenna with anisotropic substrate. The uniaxially anisotropic medium shows anisotropy of an electric type as well as anisotropy of a magnetic type. The extended spectral-domain integral equation with the Galerkin moment method solution has been used to solve for the resonant frequency, half-power bandwidth of the antenna structure. Both permittivity and permeability tensors of the anisotropic substrate have been included in the formulation of the dyadic Green's function of the problem. The accuracy of the method was checked by performing a set of results in terms of resonant frequencies for various anisotropic substrate materials. In all cases, very good agreements compared with the literature were obtained. Computations show that uniaxial electric anisotropy as well as uniaxial magnetic anisotropy affects the resonant characteristics of the rectangular antenna and consequently they must be taken into account in the design stage. The effect of electric anisotropy is more pronounced for thick substrate than for thin substrate, whereas, the effect of magnetic anisotropy is significant for thin as well as for thick substrates. The results obtained also indicate that rectangular microstrip patch on uniaxial substrate with properly selected electric and magnetic anisotropy ratios is more advantageous than the one on isotropic substrate by exhibiting wider bandwidth characteristic.

References

[1] A. MoradiKordalivand and T. A. Rahman, "Broadband modified rectangular microstrip patch antenna using stepped cut at four corners method", Progress In Electromagnetics Research, vol. 137, **(2013)**, pp. 599-619.
[2] S. Das, P. Sarkar and S. Chowdhury, "Design and analysis of a compact monitor-shaped multifrequency microstrip patch antenna", Journal of Electromagnetic Waves and Applications, vol. 28, **(2014)**, pp. 827-837.
[3] A. Kalinli, S. Sagiroglu, and F. Sarikoc, "Parallel ant colony optimization algorithm based neural method for determining resonant frequencies of various microstrip antennas," Electromagnetics, vol. 30, **(2010),** pp. 463-481.
[4] B. D. Braaten, D. A. Rogers and R. M. Nelson, "Multi-Conductor Spectral Domain Analysis of the Mutual Coupling Between Printed Dipoles Embedded in Stratified Uniaxial Anisotropic Dielectrics," IEEE Transactions on Antennas and Propagation, vol. 60, **(2012),** pp. 1886-1898.
[5] J. W. Graham and J. K Lee, "Rectangular patch antennas on biaxial substrates", IEEE Antennas and Propagation Society International Symposium (APSURSI), **(2013),** pp. 1544-1545.
[6] F. Bouttout, F. Benabdelaziz, A. Benghalia, D. Khedrouche and T. Fortaki, "Uniaxially anisotropic substrate effects on resonance of rectangular microstrip patch antenna," Electronics Letters, vol. 35, **(1999),** pp. 255-256.
[7] A. Boufrioua, A. Benghalia and F. Bouttout, "Resonant frequency of a rectangular patch antenna using asymptotic basis functions," COMPEL: The International Journal for Computation and Mathematics in Electrical and Electronic Engineering, vol. 27, **(2008)**, pp. 638-650.
[8] C. Zebiri, M. Lashab and F. Benabdelaziz, "Rectangular microstrip antenna with uniaxial bi-anisotropic chiral substrate–superstrate", IET microwaves, antennas & propagation, vol. 5, no. 1, **(2011)**, pp. 17-29.
[9] C. Zebiri, M. Lashab and F. Benabdelaziz, "Rectangular microstrip antenna with uniaxial bi-anisotropic chiral substrate–superstrate", IET microwaves, antennas & propagation, vol. 5, **(2011)**, pp. 17-29.
[10] V. Losada, R. R. Boix and M. Horno, "Resonant modes of circular microstrip patches in multilayered substrates", IEEE Transactions on Microwave Theory and Techniques, vol. 47, **(1999)**, pp. 488-498.
[11] C. Gürel and E. Yazgan, "Resonant frequency of air gap tuned circular microstrip antenna with anisotropic substrate and superstrate layers", Journal of Electromagnetic Waves and Applications, vol. 24, **(2010)**, pp. 1731-1740.
[12] S. Bedra, R. Bedra, S. Benkouda and T. Fortaki, "Full-wave analysis of anisotropic circular microstrip antenna with air gap layer", Progress In Electromagnetics Research M, vol. 34, **(2014)**, pp. 143-151.

[13] C. Vasconcelos, M. Albuquerque, G. Freitas and A. d'Assunção, "Study of a microstrip antenna on anisotropic metamaterials", Applied Physics A, vol. 111, **(2013)**, pp. 1085-1089.
[14] T. Fortaki, L. Djouane, F. Chebara and A. Benghalia, "Radiation of a rectangular microstrip patch antenna covered with a dielectric layer", International Journal of Electronics, vol. 95, **(2008)**, pp. 989-998.
[15] T. Fortaki and A. Benghalia, "Rigorous full-wave analysis of rectangular microstrip patches over ground planes with rectangular apertures in multilayered substrates that contain isotropic and uniaxial anisotropic materials", Microwave and Optical Technology Letters, vol. 41, **(2004),** pp. 496-500.
[16] F. Bouttout, F. Benabdelaziz, T. Fortaki and D. Khedrouche, "Resonant frequency and bandwidth of a superstrate-loaded rectangular patch on a uniaxial anisotropic substrate", Communications in numerical methods in engineering, vol. 16, **(2010)**, pp. 459-473.
[17] D. M. Pozar, "Microwave engineering", (John Wiley & Sons, 2009), **(2009)**.
[18] N. Aouabdia, N.-E. Belhadj-Tahar, G. Alquie and F. Benabdelaziz, "Theoretical and experimental evaluation of superstratee on rectangular patch resonator parameters", Progress In Electromagnetics Research B, vol. 32, **(2011)**, pp. 129-147.
[19] "HFSS: High Frequency Structure Simulator", Ansoft Corp, **(2011)**.
[20] D. M. Pozar, "Radiation and scattering from a microstrip patch on a uniaxial substrate", IEEE Transactions on Antennas and Propagation, vol. 35, **(1987)**, pp. 613-621.

